How Waves Affect the Distribution of Particles that Float on a Liquid Surface

P. Denissenko,[1] G. Falkovich,[2] and S. Lukaschuk[1]

[1]*Fluid Dynamics Laboratory, University of Hull, HU6 7RX, United Kingdom*

[2]*Physics of Complex Systems, Weizmann Institute of Science, Rehovot 76100, Israel*

(Received 22 November 2005; published 11 December 2006)

We study experimentally how waves affect the distribution of particles that float on a liquid surface. We show that clustering of small particles in a standing wave is a nonlinear effect with the clustering time decreasing as the square of the wave amplitude. In a set of random waves, we show that small floaters concentrate on a multifractal set with caustics.

DOI: 10.1103/PhysRevLett.97.244501 PACS numbers: 47.27.−i, 05.40.−a, 47.35.−i, 47.53.+n

Even for incompressible liquids, surface flows are generally compressible and can concentrate pollutants and floaters. Spatially smooth random flows can be characterized by the Lyapunov exponents whose sum is the asymptotic in time rate of volume change in the Lagrangian frame (comoving with the fluid). Since contracting regions contain more fluid particles and thus have more statistical weight than expanding ones, the rate is generally negative in a smooth flow (for volume in the phase space, this is a particular case of the second law of thermodynamics) [1–3]. As a result, density concentrates on a fractal (Sinai-Ruelle-Bowen) measure in a random compressible flow [1]. Indeed, it has been observed experimentally that random currents concentrate surface density on a fractal set [4–8]. Moreover, the recent theory predicts that the measure must actually be multifractal; i.e., the scaling exponents of the density moments do not grow linearly with the order [2,9,10].

Here we study the effect of clustering by waves on a liquid surface. In a single-mode standing wave, the fluid surface expands and contracts periodically. In a set of random waves, one may find regions where contractions accumulate and lead to the growth of concentration. This is true, yet for potential waves the respective rate of clustering of the points on the water surface is predicted to appear only in the sixth order in wave amplitudes [11,12]. Since the wave amplitudes are typically much less than the wavelengths (otherwise, waves break), such clustering is expected to be unobservable. For example, for waves with periods in seconds and the (pretty large) ratio of the amplitude to wavelength 0.1, the clustering time is in weeks. However, even small particles can move relative to the fluid. The physical mechanism that causes the drift of floaters relative to a water surface is the capillarity which breaks Archimedes' law and makes a floater inertial (i.e., lighter or heavier than the displaced liquid). As a result, the floaters cluster in a standing wave (either in the nodes or in the antinodes depending on the capillary sign)—a brief report of the discovery of this phenomenon has been published in [13]. It was argued theoretically that the drift must appear in the second order in the standing wave amplitude [13]. The first part of our experimental results described here shows that this is indeed the case. In the second part, we demonstrate that floaters concentrate on a multifractal set with caustics in a flow of random waves.

One can generate a stationary standing wave with well-defined boundary conditions and a controlled amplitude by a parametric instability in a vertically vibrating cell filled with a liquid [14]. Our setup is shown in Fig. 1 and is similar to that described in [15]. A cell C with the horizontal dimensions 9.6×58.3 mm and the depth 10 mm was attached to an electromagnetic shaker V, whose oscillation amplitude and frequency were controlled by a digital signal generator. The amplitude was measured by an accelerometer attached to the moving frame. To eliminate the meniscus, we used "brim-full" boundary conditions filling the cell with purified water ($R = 18$ MOhm $\cdot$ cm) precisely up to the edge of the lateral walls made from a wetting material. An aqueous suspension of particles, hydrophilic glass hollow spheres of average size 30 μm and density 0.6 g/cm^3, was added just before sealing and final level adjustment. The particles spread readily over a flat water surface and do not form stable clusters. This is possibly caused by an electrostatic repulsion of charged particles, which compensates for the attraction due to the deformation of the water surface.

The cell was illuminated from below by an expanded collimated beam (pinhole $P1$, lenses $L1$-$L2$) from 20-mW continuous He-Ne laser, CWL. The rays passing through

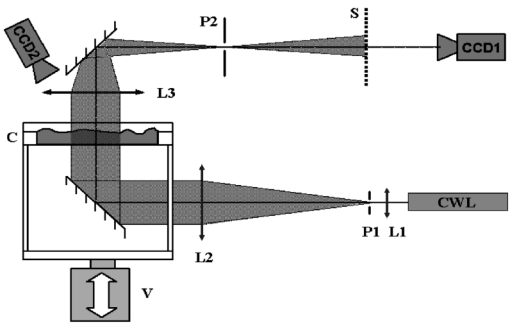

FIG. 1. Experimental setup.

the cell were refracted by waves and collected by the lens $L3$ of focal length 250 mm. We measured the amplitude of the wave through the maximum angle of the light beam refraction. For that purpose a camera (not shown) with the resolution 752×582 pixels recorded images from the screen $P2$ positioned at the focal plane of $L3$ with the shutter opened for a few periods of the wave.

The screen $P2$ had a 0.1 mm pinhole centered at the optical axis, such that the nonrefracted light passed through the pinhole and formed an image of antinodes on the screen S. That image was recorded by the camera CCD1 from Dantec PIV system with the resolution 2048×2048 pixels. An example is the top image in Fig. 2(a). The shutter of CCD1 was open for the time interval equal to one period of the wave. Appearance of the wave leads to light refraction and to a nonuniform light intensity recorded by CCD1. The variance of the light intensity from CCD1, $\mathrm{Var}(I_w)$, integrated over the entire cell was used to track the temporal evolution of the wave amplitude [see Fig. 2(b)] to pinpoint the moment when the wave starts to grow, which is necessary for the measurements of the clustering time. The camera CCD2 (with the same resolution) was used to record the particle distribution. The axis of CCD2 was inclined to the main optical axis at the angle $\simeq 10°$ to receive only the light scattered by the particles. A calibration procedure was applied to compensate image distortions due to the inclination. The shutter of CCD2 was synchronized with the phase of shaker oscillations and was opened when the liquid surface in the cell was nearly flat. Its exposure time, ~ 1 ms, was short enough to avoid particle smearing in images. An example of a typical CCD2 record is the bottom image in Fig. 2(a). Two variances of the light intensity, $\mathrm{Var}(I_{px})$ and $\mathrm{Var}(I_{py})$, measured by CCD2 characterize the inhomogeneities of the particle distribution along the x and y axes, respectively, see Figs. 2(c) and 2(d). All variances, $\mathrm{Var}(I_w)$, $\mathrm{Var}(I_{px})$, and $\mathrm{Var}(I_{py})$, characterize the inhomogeneity of the images. They are calculated by integrating the square of light intensity minus the mean intensity over the bins with the sizes listed in Fig. 2(b)–2(d) (1 pixel = 25 μm).

Let us briefly comment on the preparation of the measurements. Since we found it impossible to mix particles without destroying the surface wave pattern, our procedure included four phases: (1) a preliminary experiment where the wave pattern and a frequency corresponding to the minimum parametric instability acceleration threshold (R_c) [16] were found; (2) raising the acceleration amplitude to $R \sim 5R_c$ to effectively mix particles; (3) decreasing the acceleration amplitude to $R \sim 0.9R_c$ (i.e., below the parametric instability threshold) and letting the wave to decay; (4) again increasing the acceleration amplitude above the threshold to a desired amplitude $R_i > R_c$ and making the measurements of the wave growth and the clustering of particles. Recording images by CCD1 and CCD2 is started in the phase 4 after the amplitude is set to R_i and before the parametric wave appears. One hundred frames were collected by each camera. We did a few runs with the phases 2–4 to adjust the image acquisition rate and the time delay of the image acquisition start. Each sequence of images is started from the state with a flat liquid surface and uniformly distributed particles, so that the variance of intensity for each type of images CCD1 and CCD2 is minimal. We determine Δ_w, the standard deviation of $\mathrm{Var}(I_w)$, during that stage and register the beginning of wave growth when $\mathrm{Var}(I_w)$ grows beyond $3\Delta_w$. We call the clustering time the delay between the beginning of the growth of $\mathrm{Var}(I_w)$ and the saturation of $\mathrm{Var}(I_{px})$ (when it reaches its stationary mean value for the first time). One can see in Fig. 3 that the inverse clustering time is indeed proportional to the square of the wave amplitude, as predicted by the theory [13]. The error bars in Fig. 3 are

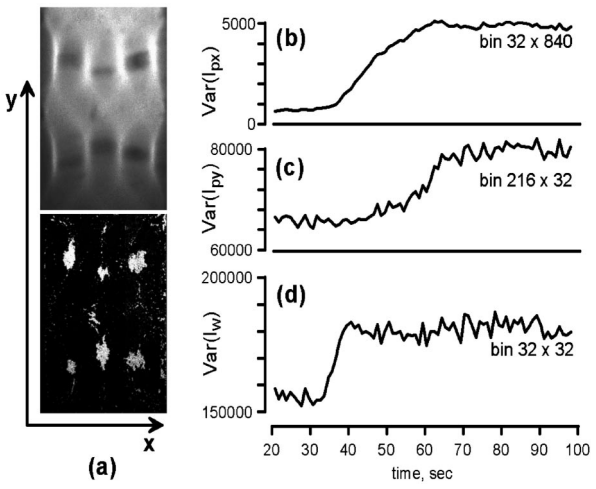

FIG. 2. The images of antinodes from CCD1 (top) and particle clusters from CCD2 (bottom) when the clustering process reached the stationary phase (a); the variances of light intensities as a function of time showing the growth of wave amplitude (b) and the growth of inhomogeneities in the concentration of particles along the x axis (c) and y axis (d).

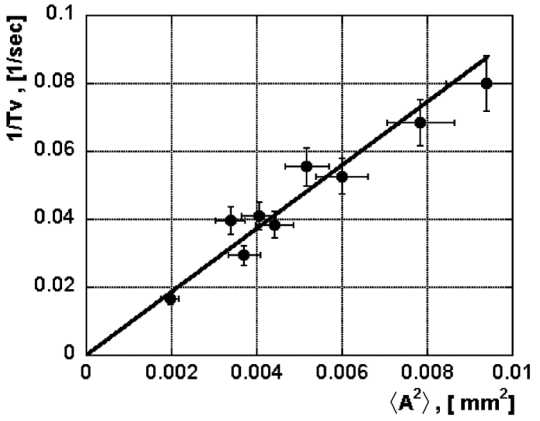

FIG. 3. The inverse time of clustering (along x axis) as a function of the squared wave amplitude. The oscillation frequency is 62.2 Hz, and the acceleration threshold of the parametric instability R_c is 459 cm/s^2.

estimated from the standard deviations of $\mathrm{Var}(I_w)$ and $\mathrm{Var}(I_{px})$ for the clustering time and from the finite precision of measuring distances and determining image boundaries at $P2$ for the amplitude.

Quasilinear standing waves exist only at small amplitudes of shaker vibrations. Increasing the amplitude one observes more and more complicated patterns, from spatiotemporal chaos to developed wave turbulence, see, e.g., [15–19]. Random compressible flows are generally expected to mix and disperse at the scales larger than the correlation scale of the velocity gradients and to produce very inhomogeneous distributions at smaller scales; see [2,3,9,11,20–22] for theory and [4–7,23,24] for experiments. Here we focus on the small-scale inhomogeneity which can be characterized as follows. Consider a number of particles inside a circle of radius r around the point $\mathbf{x}$: $n_r(\mathbf{x})$. One asks how the statistics of the random field $n_r(\mathbf{x})$ changes with the scale of resolution r. Such a change can be characterized by the scaling exponents, ζ_m, of the moments: $\langle n_r^m \rangle \propto r^{\zeta_m}$. Note that $\zeta_0 = 0$ and $\zeta_1 = 2$. When the distribution is smooth on a surface, one expects $\zeta_m = 2m$. When this equality breaks for some m, one usually calls the distribution fractal. A recent theory for a short-correlated compressible flow [2,9] gives the set of the exponents ζ_m depending nonlinearly on m, which corresponds to a multifractal distribution (those theoretical formulas give the Lagrangian exponents which in our notations are $\zeta_{n+1} - 2$). Multifractality of the measure means that the statistics are not scale invariant: strong fluctuations of particle concentration are getting more probable as one goes to smaller scales (increasing resolution). The fractal (information) dimension for a random surface flow has been measured by Sommerer and Ott, who found noninteger $d = d\zeta_m/dm|_{m=0}$ [4]. Additionally, the scaling of the second moment has been found and related to the correlation dimension (again noninteger) [5,6]. Therefore, fractality of the distribution has been established in [4–6]. To the best of our knowledge, different dimensions have not been compared for the same flow (when found different, that demonstrate multifractality as in our measurements presented below).

In the second part of the experiment we measured the moments of the concentration per unit area (defined as $n_r r^{-2}$) for the suspension of small hydrophilic particles mixed by a random flow of surface waves (at the driving amplitude $\sim 2R_c$ when it is not yet developed turbulence but rather few interacting modes that provide for a Lagrangian chaos). The experiment has been done for the set of the oscillation frequencies from 30 to 220 Hz and the amplitudes 1.8–2.5A_c. We reproduce here a typical result for the parametric wave with the frequency 32 Hz, the wavelength about 7 mm at the oscillation amplitude 198 μm $\simeq 2A_c$. A snapshot of the floaters distribution for this set is shown in Fig. 4.

The most reliable approach to quantify the particle concentration is to recognize and count individual particles. We used fluorescent microspheres with the diameter $d = 95$ μm and the density 1.05 g/cm^3 floating in 20% salt (NaCl) solution in water. Fluorescence greatly improves the image contrast, eliminates spurious refractions, and allows positioning the CCD2 camera with an optical filter on the system optical axis. In this experiment, we used a continuous wave 6 W argon ion laser (488 nm) for illumination and the bigger cell $50 \times 50 \times 10$ mm with a greater number of waves. The illumination scheme was the same as in the first part. The size of the observation area is about 30×30 mm, the pixel size 15 μm, and the particle diameter is 6.3 pixels. Prior to particle recognition the images were preprocessed. The background noise was subtracted using a threshold equal to the mean intensity plus 3 standard deviations. The resulted images were smoothed by convolution with a 5×5 pixels mask of a Gaussian shape (two-dimensional low-pass filter). The particle coordinates were determined maximizing the correlation of the image with a 3×3 mask. The method was validated by comparing the number of particles with that estimated during the emulsion preparation. The particle detection in the dense clusters was verified by direct visual inspection of images. No particle overlaps were observed. The error in the particle coordinate is less than ± 1 pixel or ± 15 μm.

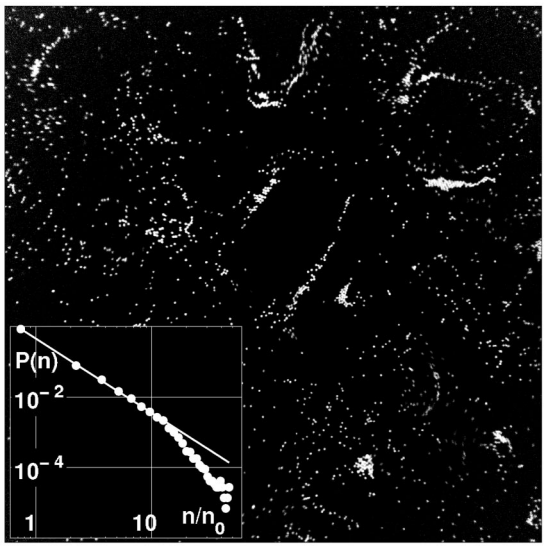

FIG. 4. A central part (20×20 mm) from a typical image of particle distribution in random waves at high mean concentration, 3.8 particles per square mm. Inset: the histogram of particle concentration in the boxes 0.96×0.96 mm at low mean concentration 1.46 particles per square mm ($n_0 = 1.35$ particles per box). The straight line is $P \propto n^{-2}$ presumably due to caustics.

Over 1000 images with particle distributions were recorded at the sampling interval 4 sec. The first six compensated moments of the coarse-grained concentration, $N_m = \langle n_r^m \rangle r^{-2m} \propto r^{\zeta_m - 2m}$, are shown in Fig. 5 versus the scale of averaging (normalized box size r/d). The bars show the standard errors. We see that indeed the moments with $m > 1$ grow when r decreases below the half wave-

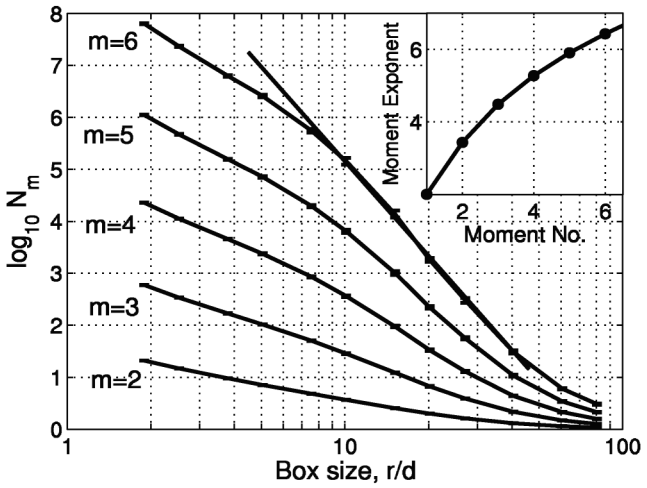

FIG. 5. Compensated moments of concentration (2–6) vs the normalized box size r/d. Inset: scaling exponents of the moments (not compensated) vs moment order.

length of the parametrically excited mode ($r/d = 40$). This growth slows down when r decreases below $r/d = 8$. This is possibly due to the dense clusters where the finite particle size, short range repulsion, and the particle backreaction on the flow are important. An additional reason may be an insufficient representation of dense regions by a finite number of particles. In the interval $8 < r/d < 40$, the data can be approximated by the straight lines which correspond to the power laws on this log-log plot. The scaling exponents are shown in the inset. The nonlinearity of the dependence of ζ on m can be interpreted as the first experimental sign of multifractality in the distribution of particles.

Another interesting aspect of the floater motion is related to inertia which may cause particle paths to intersect. This phenomenon was predicted in [25] and was called the sling effect; it must lead to appearance of caustics in the particle distribution [26]. At weak inertia (like in our system), caustics are (exponentially) rare [25,26] yet we likely see one at the center of Fig. 4. Indeed, as argued in [25], breakdowns of particle flow are mostly one-dimensional so that caustics must look locally like two parallel straight lines. One-dimensional folds in the particle distribution lead to an explosive growth of the concentration, $n \propto (t_0 - t)^{-1}$ [25], which produces a power law in the concentration probability distribution: $P(n)dn \propto dt \propto dn/n^2$. Indeed, in the inset in Fig. 4 we show the histogram of particle numbers obtained from counting particles in 2×10^5 boxes of the size 0.96×0.96 mm (64×64 pixels). The straight line corresponds to n^{-2}. Such histogram does not contain the whole information on the statistics so that our result does not rigorously prove the existence of caustics. Yet it gives strong support to the predictions of [25,26] that caustics must appear in a system of inertial particles. At higher inertia, multiple crossings of particle paths provide for extra mixing that makes the sum of Lyapunov exponents positive and the measure smooth (rather than multifractal) [27,28]. Statistical signatures of coexistence of caustics and a multifractal need further studies.

We believe that the new effect of clustering by waves is of fundamental interest in physics and might be of practical use for particle separation, cleaning of liquid surfaces, and better understanding of environmental phenomena associated with the wave transport.

The work was supported by the Royal Society, Israel Science Foundation, and Einstein Center. We thank V. Steinberg for useful discussions and V. Vladimirov for support.

[1] D. Ruelle, J. Stat. Phys. **85**, 1 (1996); **95**, 393 (1999).
[2] E. Balkovsky, G. Falkovich, and A. Fouxon, Phys. Rev. Lett. **86**, 2790 (2001).
[3] G. Falkovich, K. Gawedzki, and M. Vergassola, Rev. Mod. Phys. **73**, 913 (2001).
[4] J. C. Sommerer and E. Ott, Science **259**, 335 (1993).
[5] J. C. Sommerer, Phys. Fluids **8**, 2441 (1996).
[6] A. Nameson, T. Antonsen, and E. Ott, Phys. Fluids **8**, 2426 (1996).
[7] J. Cressman and W. Goldburg, J. Stat. Phys. **113**, 875 (2003).
[8] J. Cressman *et al.*, New J. Phys. **6**, 53 (2004).
[9] J. Bec, K. Gawedzki, and P. Horvai, Phys. Rev. Lett. **92**, 224501 (2004).
[10] G. Boffetta, J. Davoudi, and F. De Lillo, nlin.CD/0510062.
[11] A. Balk, G. Falkovich, and M. Stepanov, Phys. Rev. Lett. **92**, 244504 (2004).
[12] M. Vucelja, G. Falkovich, and A. Fouxon, nlin.CD/0612001.
[13] G. Falkovich *et al.*, Nature (London) **435**, 1045 (2005).
[14] M. Faraday, Phil. Trans. R. Soc. London **121**, 319 (1831).
[15] B. Gluckman, C. Arnold, and J. Gollub, Phys. Rev. E **51**, 1128 (1995).
[16] S. Douady, J. Fluid Mech. **221**, 383 (1990).
[17] V. Zakharov, V. L'vov, and G. Falkovich, *Kolmogorov Spectra of Turbulence* (Springer, New York, 1992).
[18] W. Wright *et al.*, Science **278**, 1609 (1997).
[19] M. Brazhnikov *et al.*, Europhys. Lett. **58**, 510 (2002).
[20] K. Herterich and K. Hasselmann, J. Phys. Oceanogr. **12**, 704 (1982).
[21] A. Balk and R. McLaughlin, Phys. Lett. A **256**, 299 (1999).
[22] B. Eckhardt and J. Schumacher, Phys. Rev. E **64**, 016314 (2001).
[23] R. Ramshankar, D. Berlin, and J. Gollub, Phys. Fluids A **2**, 1955 (1990).
[24] E. Schröder *et al.*, Phys. Rev. Lett. **76**, 4717 (1996).
[25] G. Falkovich, A. Fouxon, and M. Stepanov, Nature (London) **419**, 151 (2002).
[26] M. Wilkinson and B. Mehlig, Europhys. Lett. **71**, 186 (2005).
[27] J. Bec, J. Fluid Mech. **528**, 255 (2005).
[28] B. Mehlig and M. Wilkinson, Phys. Rev. Lett. **92**, 250602 (2004).